Proceedings of IMECE2008
2008 ASME International Mechanical Engineering Congress and Exposition
October 31-November 6, 2008, Boston, Massachusetts, USA

IMECE2008-67973

SPECIAL MATRICES AND SHAPE FACTORS FOR LINEAR EMPIRICAL SIMILITUDE METHOD

Srikanth Tadepalli
Department of Mechanical Engineering
The University of Texas at Austin
Austin, TX 78712
512 – 762 – 0247
tsrikanth@mail.utexas.edu

Kristin L. Wood
Department of Mechanical Engineering
The University of Texas at Austin
Austin, TX 78712
512 – 471 – 0095
wood@mail.utexas.edu

ABSTRACT
Empirical Similitude Method (ESM) is a technique developed to enhance the applicability of similarity methods to incorporate more realistic experimental data and scaling effects. Much of the development has been motivated by the premise of forging a relationship between experiential information and physical systems that have inherent non – linear variables and factors affecting their response. We augment this procedure by incorporating the Toeplitz and Hankel matrices, and solve the modified linear ESM problem using the conjugate gradient method, highlighting the potential benefits in the process. A simple deflection example is illustrated for lucidity and a comparison is made between all the available methods for contrast. A final extension into the use of shape factors is made using a numerical example.

INTRODUCTION
Scaling and similarity methods stem from the idea of similitude introduced by [Rayliegh, 1915] where a complex system can be represented by an *equivalent* simpler model that is more readily analyzable. Such an approximation allows for easier experimentation of the model, the resulting test data of which can then be accurately and reliably scaled and transformed to the actual system (product). Buckingham [Bridgman, 1931] provided the initial framework to carry out such a scaling and detailed the development of the transformation process through the use of dimensionless π groups. Considering the fact that the applicability of this process is determined by the ability to determine the constants and the exponents of the scaling factors [Szirtes, 2003], the technique is limited by the degree of non – linearity and independence of the affecting geometric and material variables. While some headway can still be expected using more advanced methods, the associated experimental and computational effort also compounds relatively. In an effort to ease this effort, the ESM process [Cho, 1999] was developed that simplified the conversion by disassociating geometry and material properties and provided a means for independent individual scaling.

NOMENCLATURE
Xms – Model specimen state vector
Xps – Product specimen state vector
Xm – Model state vector
Xp – Product state vector
F – Form matrix
S – Shape matrix
T – System matrix

BACKGROUND INFORMATION
Development of rapid prototyping (RP) techniques have allowed for the fabrication of the most intricate designs. Using the leverage that Selective Laser Sintering (SLS) and other RP processes have provided, geometric constraints not being an impediment, similitude models can be developed for certain material forms like polymers and soft metals. These models can then be extended to incorporate behavior of common engineering materials and systems. The primary motivation therefore is to couple the advantage of precise fabrication and testing, to enhance similarity studies. [Cho, 1998] and [Dutson, 2002] identified the limitations of Buckingham π theorem in their effort to enhance the technique to non – linear domains. The main hypothesis of ESM is to assume that the prediction equation for any parameter of interest *P* can be written as

$$P = f_1(Scale) * f_2(Form) \quad (1)$$

for null boundary and initial conditions, and steady – state analysis. Put in a mathematical form, the method assumes that the geometric (form) and the material properties (scale) are not interrelated. [Wood, 2002] gave another expression by modifying the relation to

$$P = f_1(Scale) * f_2(Form) + R(Scale, Form) \quad (2)$$

where $R(Scale, Form)$ represents the error in the system which needs to be minimized with an appropriate choice of f_1 and f_2 [1].

The idea behind this method is to use the original mapping theorem (Buckingham π theorem) as a two stage process rather than one, where the two stages account for the individual and independent scaling of geometry and material. This necessitates the use of *three* representative geometries instead of *one* in the original concept. These geometries are referred to as the *model* (same as before), which has the same shape as the *product* but is of a different material, the *product specimen* which is a simplified geometry made of the same material as the *product* and the *model specimen* which is of the same shape as the *product specimen* but is made of the material that the *model* is made of. Shown below is an illustration of the process (see Figure 1). Such a simplification allows for the product state vector to be interpreted as

$$x_p = f(x_m, x_{ps}, x_{ms}) \tag{3}$$

where the state vectors of the model specimen, the model, the product specimen and the product are respectively given by $\boldsymbol{x_{ms}}$, $\boldsymbol{x_m}$, $\boldsymbol{x_{ps}}$, and $\boldsymbol{x_p}$. The parameters *S* and *F* are matrices that capture the geometry (form) and the material (scale) changes in the system. The product of these two matrices is the net system transformation. This allows for the evaluation of the product response at every point *i* in its domain based on the values in the other three geometries measured at the same corresponding point. Such an evaluation thus circumvents the necessity to obtain a governing equation to describe the engineering process and focuses on the estimation of the parameter through experimental (more realistic) and numerical transformations.

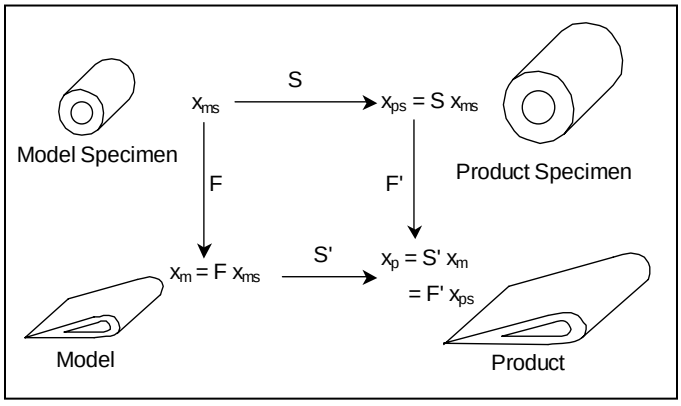

Figure 1. Empirical Similarity Method, Adapted from [Cho, 1999]

Hence, the *scale* equation takes the form given by

$$x_{ps} = Sx_{ms} \tag{4}$$

and the *form* equation is written as

$$x_m = Fx_{ms} \tag{5}$$

The product is assumed to have a variation *w.r.t* the model that is similar to equation (4) and hence the prediction equation is now developed to be

$$x_p = Sx_m = (S \times F)x_{ms} \tag{6}$$

The ability to make an accurate prediction for the product state vector is dependent now on the precise evaluation of the parameters *S* and *F*. Note that equations (4) and (5) are linear equations that are ill – conditioned as the state variables are plain column vectors while the transformation matrices have to be square for mathematical correctness. To solve such a system of equations different techniques have been embraced each of which is described in the next section along with the development of the Toeplitz and Hankel forms.

LINEAR METHODS

Several linear methods have been adopted for scaling in ESM and have provided valuable insights into the underlying engineering phenomena. To invoke these methods, we need to know apriori[2] if the product would behave linearly or not. This vital piece of information can be extracted from the test data of the specimens and the model. The trends and the distribution of the experimental results are pretty good indicators of the expected response of the product as all inherent affecting factors (geometry, material and boundary conditions) are accounted for. An example is shown below along with the working procedure of each technique to inductively illustrate the idea of mapping in the linear range. The product studied is a simple USB clip[3] (see Figure 2) whose deflection is estimated for a force applied at its free ends (for unlatching from the lock position). Since the product is symmetric about the *x* – plane, a ½ section is modeled and analyzed (see Figure 3). The specimen used is also shown (see Figure 4). The test data from the actual analysis is used to highlight every method for the *scale* transformation. The same logic holds for the *form* transformation as well.

Figure 2.1. USB Clip

[1] The method uses the linear regression model explained later in the paper.

[2] The prior knowledge of the system helps the designer with the choice of technique to use and implement.

[3] The example is a good choice for small angle deflections.

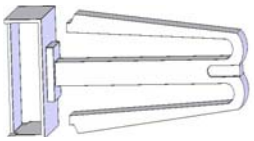

Figure 2.2. USB Clip

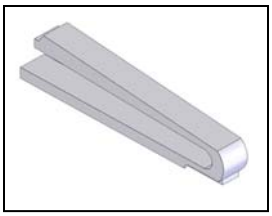

Figure 3. USB Clip ½ section

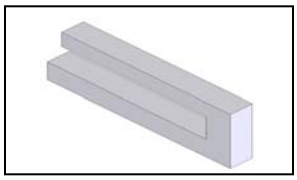

Figure 4. USB Clip Specimen

T
he first step in the analysis is to establish the linear working range of the clip deflection without testing the actual product itself. The other three representative geometries are thus analyzed using ABAQUS^{TM} software for different values of force applied to the free end and the associated deflection is plotted (see Figure 5). Notice that all three geometries show a linear trend but with different slopes as one would expect due to changing shapes, sizes and material properties. We can thus safely conclude that the product would behave linearly as well and using the linear methods to solve for the required parameter of interest is a valid approach.

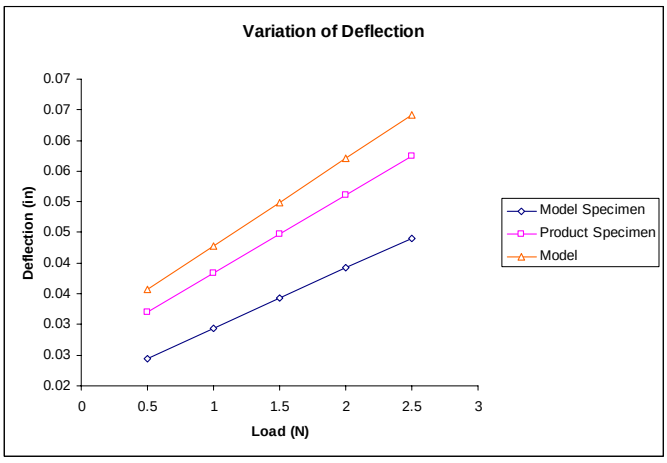

Figure 5. Test data from Representative Geometries

The classic ESM scaling equation for geometric properties necessitates

$$\{X_{ps}\} = [S]\{X_{ms}\} \tag{7}$$

The first method described to capture this transformation is the *diagonal matrix* (DM) [Dutson, 2002] approach. In this method, *i* denoting a point in the domain of the geometry, the scaling is assumed to be a simple ratio given by

$$\{X_{ps,i}\} = S\{X_{ms,i}\} \ \forall i \tag{8}$$

where *S* is given by

$$S \equiv \begin{bmatrix} s_1 & 0 & 0 .... \\ 0 & s_2 & 0 \\ 0 & 0 & s_3 \\ . & & \\ . & & \end{bmatrix} = \begin{bmatrix} \frac{X_{ps,i}}{X_{ms,i}} \end{bmatrix} \ \forall i \tag{9}$$

Using the test deflection (*in*) data from the analysis for the model specimen and the product specimen, we have,

$$X_{ms} = \begin{bmatrix} 0.0244947 \\ 0.0293936 \\ 0.0342925 \\ 0.0391915 \\ 0.0440904 \end{bmatrix}, X_{ps} = \begin{bmatrix} 0.0319442 \\ 0.038333 \\ 0.0447218 \\ 0.05111 \\ 0.0574995 \end{bmatrix}$$

which gives the scale transformation matrix to be

$$S_{DM} = \begin{bmatrix} 1.89878 & 0 & 0 & 0 & 0 \\ 0 & 1.89878 & 0 & 0 & 0 \\ 0 & 0 & 1.89878 & 0 & 0 \\ 0 & 0 & 0 & 1.89875 & 0 \\ 0 & 0 & 0 & 0 & 1.89876 \end{bmatrix}$$

In the second approach, the *pseudo – inverse* (PI) technique, the scale transformation is determined by

$$S_{PI} = X_{ps} X_{ms}^{+} \tag{10}$$

where $X_{ms}^{+} = (X_{ms}^{*} X_{ms})^{-1} X_{ms}^{*}$ [Penrose, 1955] and X_{ms}^{*} is the conjugate transpose of X_{ms}. The generated scale matrix S_{PI} now has the form

$$\begin{pmatrix} 0.127856 & 0.153427 & 0.178998 & 0.204569 & 0.23014 \\ 0.153427 & 0.184112 & 0.214797 & 0.245483 & 0.276168 \\ 0.178998 & 0.214797 & 0.250597 & 0.286397 & 0.322196 \\ 0.204567 & 0.24548 & 0.286393 & 0.327306 & 0.368219 \\ 0.23014 & 0.276168 & 0.322196 & 0.368224 & 0.414252 \end{pmatrix}$$

Notice that there is lot more system interaction captured in the pseudo – inverse approach matrix than in the diagonal matrix. This system interaction can be physically interpreted as the residual stress (or strain) in the system after a force has been applied and released. But this method is constrained by the fact that a true inverse is not generated as the original equation

(7) is improperly formed. For a true inverse, we need to invert a square matrix that guarantees a unique solution [Bernstein, 2005] and hence the circulant matrix approach (CM) has been developed [Cho, 1999]. In this process, the original equation is modified to a more useful form by invoking the circulant operator which converts a column vector[4] $[c_0 \ldots c_{n-1}]^*$ to a square matrix using the notation [Davis, 1979],

$$\begin{bmatrix} c_0 & c_{n-1} & \cdots & c_2 & c_1 \\ c_1 & c_0 & c_{n-1} & & c_2 \\ \vdots & c_1 & c_0 & \ddots & \vdots \\ c_{n-2} & & \ddots & \ddots & c_{n-1} \\ c_{n-1} & c_{n-2} & \cdots & c_1 & c_0 \end{bmatrix}$$

which then gives

$$circ[X_{ps}] = circ[S]circ[X_{ms}]$$

or
$$circ[S] = circ[X_{ps}]circ[X_{ms}]^{-1} \quad (11)$$

The scale matrix in this case is given by

$$\begin{pmatrix} 1.30413 & -1.24208\times10^{-6} & -1.24232\times10^{-6} & 0.0000285771 & -0.0000298199 \\ -0.0000298199 & 1.30413 & -1.24208\times10^{-6} & -1.24232\times10^{-6} & 0.0000285771 \\ 0.0000285771 & -0.0000298199 & 1.30413 & -1.24208\times10^{-6} & -1.24232\times10^{-6} \\ -1.24232\times10^{-6} & 0.0000285771 & -0.0000298199 & 1.30413 & -1.24208\times10^{-6} \\ -1.24208\times10^{-6} & -1.24232\times10^{-6} & 0.0000285771 & -0.0000298199 & 1.30413 \end{pmatrix}$$

Notice the smoothing effect caused by the use of the entire column vector and thus the capture of true interaction of all deflection components. This method though is hindered by the possibility of having to invert stiff or large matrices. Based on the limitations of the three methods, there exists a need for using matrices and methods that

i) Capture element interactions.
ii) Are Square in definition.
iii) Generate a true inverse.
iv) Are either not stiff or can be still used with advanced methods when stiff.

Based on these requirements, two special matrices are invoked – the Toeplitz Matrix [Grenander et al, 1958,] given by

$$\begin{bmatrix} a_0 & a_{-1} & a_{-2} & \cdots & \cdots & a_{-n+1} \\ a_1 & a_0 & a_{-1} & \ddots & & \vdots \\ a_2 & a_1 & \ddots & \ddots & \ddots & \vdots \\ \vdots & \ddots & \ddots & \ddots & a_{-1} & a_{-2} \\ \vdots & & \ddots & a_1 & a_0 & a_{-1} \\ a_{n-1} & \cdots & \cdots & a_2 & a_1 & a_0 \end{bmatrix}$$

for a column vector $[a_0 \ldots a_{n-1}]^*$ and the Hankel matrix [Peller, 2003] given by

$$\begin{bmatrix} a & b & c & d & e \\ b & c & d & e & f \\ c & d & e & f & g \\ d & e & f & g & h \\ e & f & g & h & i \end{bmatrix}$$

for a column vector $[a,b,c,d,e]^*$. Notice that Hankel matrix is the inverted (upside down) Toeplitz Matrix and the circulant matrix is a special case of the Toeplitz Matrix. The Hankel matrix generates a sparse matrix because the entries in the first column are not completely reproduced[5]. In order to solve the linear ESM problem using these two special matrices, we need to modify the scale (and form) equation –

- To generate an equation that is of the standard $Ax = b$ linear form.
- To use standard software like Matlab™ and Mathematica™ where a row vector needs to be given as an input to generate the associated Toeplitz and Hankel forms.
-

Given these constraints we modify the scale equation $[X_{ps}] = [S][X_{ms}]$ using the transpose operator such that

$$T([X_{ms}]^*)[S]^* = T([X_{ps}]^*) \equiv Ax = b \quad (12)$$

where *T* is the Toeplitz operator which is replaced by *H* to indicate the Hankel operator. Hence for a model specimen vector given by

$$X_{ms} = \begin{bmatrix} 0.0244947 \\ 0.0293936 \\ 0.0342925 \\ 0.0391915 \\ 0.0440904 \end{bmatrix}$$

[4] * indicates the transpose operator

[5] Notice that additional elements are created in the matrix (*f*, *g*, *h* and *i*) which are defaulted to zero [Peller, 2003].

the Toeplitz and the Hankel forms are respectively given by

$$T(X_{ms}) = \begin{bmatrix} 0.0245 & 0.0294 & 0.0343 & 0.0392 & 0.0441 \\ 0.0294 & 0.0245 & 0.0294 & 0.0343 & 0.0392 \\ 0.0343 & 0.0294 & 0.0245 & 0.0294 & 0.0343 \\ 0.0392 & 0.0343 & 0.0294 & 0.0245 & 0.0294 \\ 0.0441 & 0.0392 & 0.0343 & 0.0294 & 0.0245 \end{bmatrix}$$

$$H(X_{ms}) = \begin{bmatrix} 0.0245 & 0.0294 & 0.0343 & 0.0392 & 0.0441 \\ 0.0294 & 0.0343 & 0.0392 & 0.0441 & 0 \\ 0.0343 & 0.0392 & 0.0441 & 0 & 0 \\ 0.0392 & 0.0441 & 0 & 0 & 0 \\ 0.0441 & 0 & 0 & 0 & 0 \end{bmatrix}$$

While the first three requirements have been satisfied, the need to compute the inverse when stiff conditions are encountered still persists with these matrices. Hence, we use the *conjugate gradient* method [Shewchuk, 1994] that works with the idea of minimizing residuals[6] when computing inverses and allows for small perturbations[7] being a numerical procedure. The basic scale equation is now modified to

$$\begin{aligned} T\left(\left[X_{ms}\right]^{*}\right)\left(\left[S\right]_{CG}^{*}\right) &= T\left(\left[X_{ps}\right]^{*}\right) \\ H\left(\left[X_{ms}\right]^{*}\right)\left(\left[S\right]_{CG}^{*}\right) &= H\left(\left[X_{ps}\right]^{*}\right) \end{aligned} \tag{13}$$

Solving these linear equations using the conjugate gradient method generates the required scale transformation matrices respectively given by

$$\begin{bmatrix} 1.30413 & -6.21249\times10^{-6} & -8.86868\times10^{-7} & 0.0000683369 & -0.0000725532 \\ -2.23057\times10^{-9} & 1.30413 & -9.0512\times10^{-12} & -0.0000745487 & 0.000145993 \\ -0.0000745479 & -6.34065\times10^{-10} & 1.30413 & -6.34065\times10^{-10} & -0.0000745479 \\ 0.000145993 & -0.0000745487 & -9.05133\times10^{-12} & 1.30413 & -2.23057\times10^{-9} \\ -0.0000725532 & 0.0000683369 & -8.86868\times10^{-7} & -6.21249\times10^{-6} & 1.30413 \end{bmatrix}$$

and

$$\begin{bmatrix} 1.30413 & 4.44089\times10^{-16} & -6.45981\times10^{-9} & -2.83334 & -1.23165\times10^{-16} \\ -0.0000161064 & 1.30413 & 0.0274868 & -8.58844 & 5.62037\times10^{-16} \\ 0.0000145467 & -0.0000161064 & 1.27664 & 18.6752 & 2.91542\times10^{-16} \\ -4.03258\times10^{-7} & 0.0000145467 & -0.0000147333 & -6.17442 & -1.62427\times10^{-16} \\ -4.47995\times10^{-7} & -4.03258\times10^{-7} & 4.4785\times10^{8} & 211808. & 1.30413 \end{bmatrix}$$

Notice that even though some of the elements in the model specimen vector are numerically small, an inverse is still obtained as the method allows for minor perturbations. The same process is now repeated in estimating the form transformation matrix *F* for each method. Modifying the prediction equation accordingly to incorporate the Toeplitz and Hankel forms, we have

$$\begin{aligned} T\left[X_p\right] &= \left[S\times F\right]T\left[X_{ms}\right] \\ H\left[X_p\right] &= \left[S\times F\right]H\left[X_{ms}\right] \end{aligned} \tag{14}$$

where we have made use of the identity

$$S\times F = (F^{*}\times S^{*})^{*} \tag{15}$$

Note that only the first column of the end results includes values of interest as other columns are artificially introduced by the Toeplitz and Hankel operators. Before we proceed to compare the values against the first three methods a final method is shown which uses the linear regression process to estimate the scale and form transformations. Developed by [Wood, 2002], the scale and form transformations are obtained using a linear best fit curve to approximate the test data. The mathematical description for the scale transformation is shown below.

$$\begin{aligned} &\left[X_{ps}\right] = \left[1 \;\; X_{ms}\right]\left[v\right] \\ &\Rightarrow \begin{bmatrix} X_{ps,1} \\ X_{ps,2} \\ . \\ . \end{bmatrix} = \begin{bmatrix} 1 & X_{ms,1} \\ 1 & X_{ms,2} \\ . & \\ . & \end{bmatrix}\begin{bmatrix} a \\ b \end{bmatrix} = \left[Z_{ms}\right]\begin{bmatrix} a \\ b \end{bmatrix} \end{aligned} \tag{16}$$

where *a* and *b* are the coefficients of the best fit curve given by

$$\begin{bmatrix} a \\ b \end{bmatrix} = \left[X_{ps}\right]Z_{ms}^{+} \tag{17}$$

where Z_{ms}^{+} is the pseudo – inverse of the compensated matrix (Comp. M). Hence, the prediction equation now is given by

$$\left[X_p\right] = \left[1 \;\; X_m\right]\begin{bmatrix} a \\ b \end{bmatrix} \tag{18}$$

Using the methods defined above the results of analysis is shown below. Notice that the predicted plot (see Figure 6) is close to the actual plot and all methods generate values that are very close to each other (see Figure 7). The RMS error is chosen as the error indicator to account for possible generation of negative errors. Further all observations are averaged so that a system mean can be devised. The RMS error across all the methods is about the same level at an average of 2.85% with change occurring only in the fourth decimal. To conclude this part of the analysis, a comprehensive evaluation is made in all the methods for three different criteria that capture the effectiveness of each technique (see Table 1). Notice that the newer methods provide more benefits as we can capture system interactions, observe and isolate stiff behavior and generate true and unique solutions without compromising on

[6] A residual is defined as the error between the expected and the obtained value in a particular norm.

[7] The perturbations are minor numerical adjustments made to account for probable stiff behavior.

the strict accuracy requirements achieved by earlier methods. Having established the feasibility of the Toeplitz and the Hankel matrices used in conjunction with the conjugate gradient method, we now enhance the processes by evaluating another numerical example where we study and incorporate shape factors to influence ESM analysis.

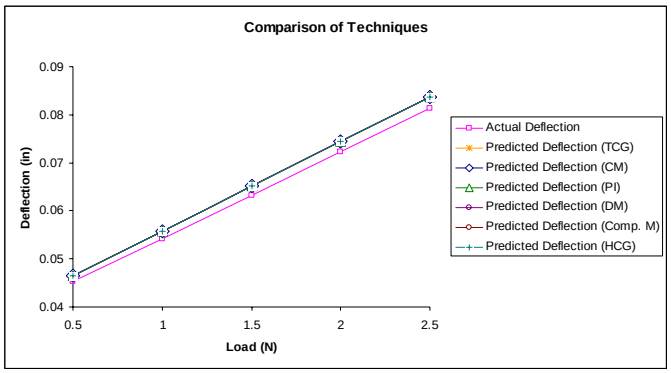

Figure 6. Prediction Plot

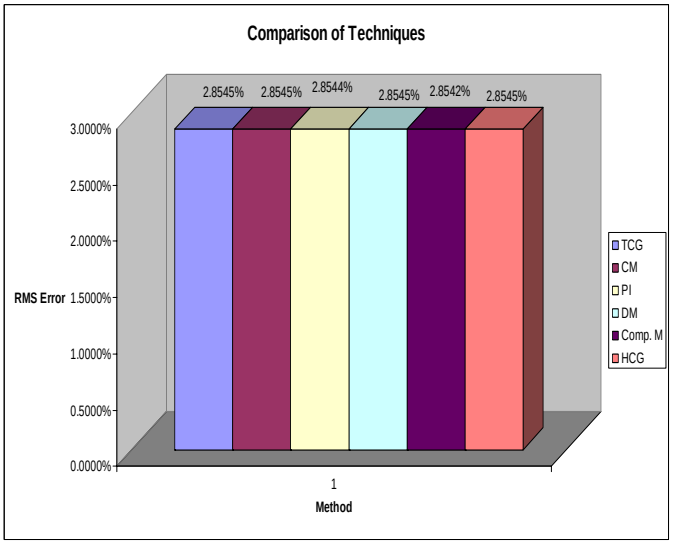

Figure 7. Error Comparison

Table 1. Comparison of Methods

Technique	Error	System Interactions	Robustness
Diagonal Matrix	2.8545%	No	Possible numerical error due to small values
Pseudo Inverse	2.8544%	Partial	Not true inverse
Circulant Matrix	2.8545%	Yes	Possible stiffness in matrices
Compensation Matrix	2.8542%	Yes	Highly accurate
Toeplitz - CG*	2.8545%	Yes	Highly robust and accurate
Hankel - CG*	2.8545%	Yes	Highly robust and accurate

SHAPE FACTORS

[Ashby, 1991] defines shape factors as the "*Dimensionless numbers that characterize the efficiency of a section shape, regardless of scale, in a given mode of loading*". Shape factors though, are not restricted to mechanics of solids and are widely used in fluid and thermal systems [Incropera, 2007]. They manifest in different forms in the engineering world as correction factors to account for changes in different input, boundary or geometric conditions.

Building on the analysis of the previous example where we presented a choice of specimen that was judiciously selected based on the geometry of the clip, in this section we introduce the effect of shape factors in ESM studies. The incorporation of shape factors in ESM holds special significance in terms of specimen scaling. Ideally, a single specimen choice should suffice the need for experimental similitude but the choice of such a specimen needs to be done based on justified reasoning and technical argument. Conjuring up a specimen is not a trivial task and hence the need for exploring different specimen geometries that represent the actual system. Hence if ϕ represents the shape factor for a particular geometry, then the ESM prediction equation is modified to

$$x_p = \phi_e (S \times F) x_{ms} \tag{19}$$

where the shape factor $\phi_e = \dfrac{\phi_{specimen}}{\phi_{model}}$ accounts for the dissimilarity between the specimen shape and the actual geometry. For any solid, the dimensionless and unit less shape factor is defined for bending and buckling modes to be [Ashby, 1992]

$$\phi = \frac{4\pi I}{A^2} \tag{20}$$

where I is the second area Moment of Inertia and A is the cross – sectional area. Bear in mind that these shape factors are characteristics of mechanical domain alone and will vary for thermal or other systems. For regular geometries with one characteristic dimension (circle, square), the shape factor

reduces to a fixed constant but for a geometry like an ellipse which has two characteristic dimensions, the shape factor is variable and is given by the ratio of the two dimensions.

$$\phi_{cir} = \frac{4\pi I_{cir}}{A_{cir}^2} = 4\pi\left(\frac{\pi r^4}{4}\right)\left(\frac{1}{\pi^2 r^4}\right) = 1$$
$$\phi_{sq} = \frac{4\pi I_{sq}}{A_{sq}^2} = 4\pi\left(\frac{b^4}{12}\right)\left(\frac{1}{b^4}\right) = \frac{\pi}{3} \quad (21)$$
$$\phi_{elp} = \frac{4\pi I_{elp}}{A_{elp}^2} = 4\pi\left(\frac{\pi a^3 b}{4}\right)\left(\frac{1}{\pi^2 a^2 b^2}\right) = \frac{a}{b}$$

Based on this initial research on shape factors several conclusions can be safely derived –

i) Shape factors are primarily geometric features that define how well a geometry approximates another.
ii) Shape factors are functions of geometry alone.
iii) Shape factors are domain and application dependent.
iv) Shape factors are either fixed or variable depending on the type of cross – section.
v) Shape factors are functions of the characteristic dimensions that define the cross – section.

Like before we present the effect of shape factors in ESM inductively using an example where we analyze the vertical deflection of an interconnect, a device that mechanically and electrically connects a chip package to the board that they are mounted on [Harper, 2005], for a compressive load of 10N. Based on the technology developed by IBM[8], these devices are responsible for a fixture between two different geometries and provide very tight tolerances. The traditional design of an interconnect is shown below.

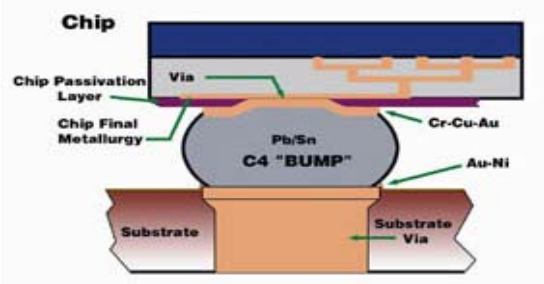

Figure 8. A typical interconnect geometry

The geometry involves a bottle like structure with a neck region. Compressive forces are applied on the top causing stress in the structure. Since the neck region is the weakest, fracture occurs at the neck ('*C*') causing improper electrical and mechanical connectivity. To analyze this problem, several approaches have been used in the industry with Finite Element Methods (FEM) [Becket et al, 1981] playing a major role in the evaluation.

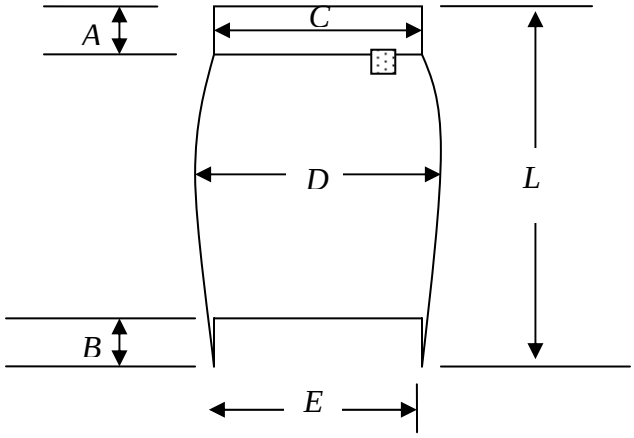

Figure 9. A typical interconnect geometry with dimensions

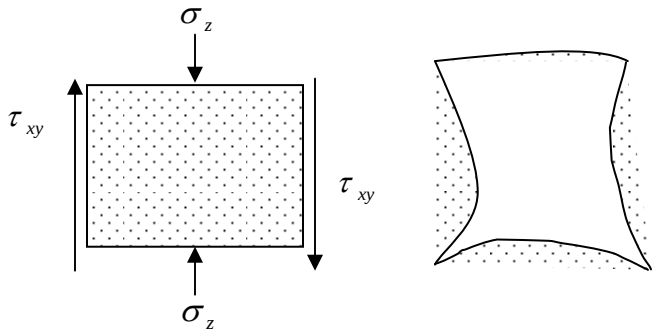

Figure 10. Stress element and deformed stress element

A typical stress element in the geometry at the neck region involves a structure that is subjected to normal compressive stresses and tangential shear stress causing a net deformation as shown above. Since the normal deformations have higher numerical precedence, the vertical deflection of the element is considered as the failure mode for analysis in this paper.

This geometry is rather difficult to analyze due to its relative complexity and hence is pertinent to ESM as it involves geometric and parametric distortion while using multiple materials (Pb/Sn alloy). The three specimens that are analyzed are shown below (see Figure 11). The geometric distortion arises from the fact that the section involving the dimension '*B*' is modeled as a continuous structure and the cross – section at the neck, '*C*' varies from tapered circle in the product to square, circular and elliptical in the specimens. Also, in order to maintain consistency in scaling the aspect ratio, the three structures provide a rather simple selection. Further, the analysis would need to incorporate the scaling in measurement location '*A*', which causes the parametric distortion. The three specimens selected are based on the need to maintain length and width consistency while ensuring surface contact between the load delivering medium (package) [Pecht et al, 1999] and the load bearing surface of the

[8] http://www- 03.ibm.com/chips/about/technology/makechip/interconnect/4.html

interconnect. Since the deflection at the neck level is analyzed, the stress zones are concentrated in this region. The deflection is estimated using the Toeplitz and Hankel matrix methods for a force input.

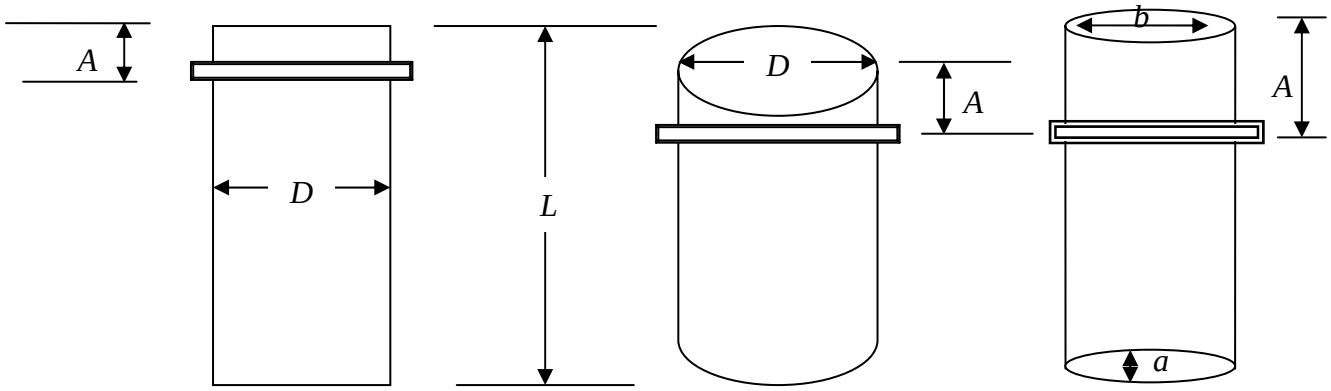

Figure 11. Specimen for Shape Factor analysis

Table 2. Specimen Shape Factors

Geometry	Domain	Application	Fixed	$\phi_{specimen}$
Cylinder	Solids	Buckling	Yes	1
Square	Solids	Buckling	Yes	$\frac{\pi}{3}$
Ellipse	Solids	Buckling	No	$\frac{a}{b}$

Table 3. Geometric data

Product			Model		
a	5	Micron	***a***	2.5	micron
b	3.05	Micron	***b***	1.525	micron
C	20	Micron	***C***	10	micron
D	28.28	Micron	***D***	14.14	micron
E	10	Micron	***E***	5	micron
L	33.23	Micron	***L***	16.615	micron
P	10	N	***P***	10	N

Table 4. ESM Shape Factors

Geometry	ϕ_{model}	ϕ_e
Cylinder	1	1
Square	1	$\frac{\pi}{3}$
Ellipse	1	0.6944

Table 5. Material Data

Geometry	Scale	Load (N)	Material	Material Properties	
				E	υ
Product	1	10	37/63 Pb/Sn Alloy	37.5 GPa	0.38
Product Specimens	1	10	37/63 Pb/Sn Alloy	37.5 GPa	0.38
Model	0.5	10	Nylon[9]	19.1 GPa	0.35
Model Specimens	0.5	10	Nylon	19.1 GPa	0.35

The analysis is again performed using ABAQUS™ for a compressive load of 10N on all geometries. The values of deflection are estimated at uniform intervals along the *x* – direction starting from the center and proceeding towards the edge in the neck region alone. Like before, the scale and form transformation matrices are developed and the prediction estimates generated for the product. The obtained values are scaled by the respective shape factors [Ashby, 1992] that are tabulated (see Table 4) to generate the final predicted values. Note that the shape factors are for the neck region alone as this is the zone where hypothetical failure occurs. Notice that the product is approximated closely by the cylinder and not as much by the ellipse or the square. This is a clear indicator that closer the shape resemblance with the actual product better the prediction. Further, increase in error in the square cross – section can be attributed to the fact that the number of

[9] **Nylon 66, 60% Glass Fiber Filled**

boundaries rises to 4 in comparison with the cylinder (1), which conforms significantly to the actual system. The ellipse should have performed better when compared to the square but the skewness of the cross – section as defined by the ratio $\frac{a}{b}$ (also the shape factor) makes it a bad choice. Thus, there exists a need to maintain close geometric proximity with the actual system for better similarity results.

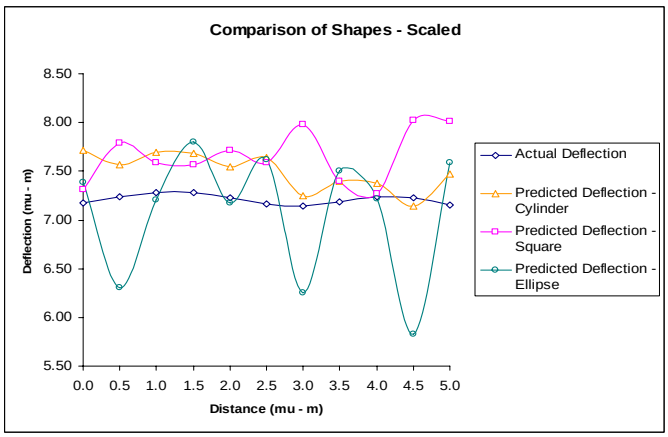

Figure 12. Comparison of Shapes

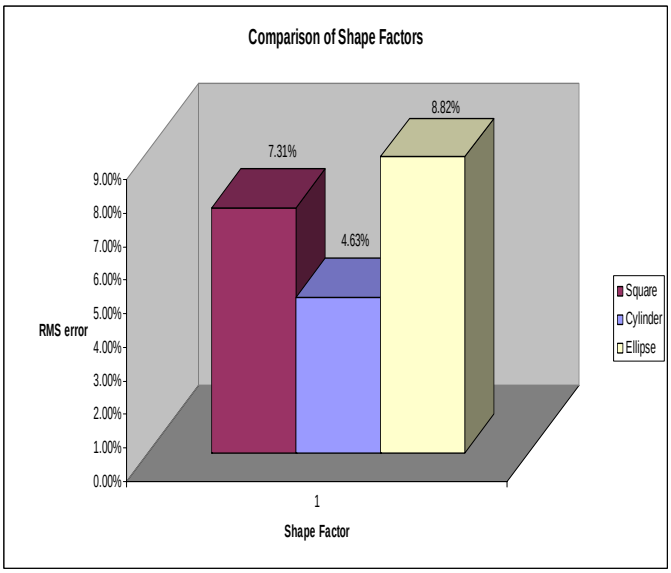

Figure 13. Errors due to Shape factors

SUMMARY

The ESM method has greatly enhanced the mathematical prediction capabilities to incorporate distinct material behavior and complex geometries. Coupled with the use of modern linear systems analysis, the technique has provided for similarity evaluation of such designs as the USB clip and the interconnect. This paper has extended the existing methodology by introducing and implementing the Toeplitz and Hankel matrix approach used in conjunction with the conjugate gradient method. Further, the application of shape factors in the evaluation of specimens and their implication in ESM has been highlighted. We present a summary of the ESM process from a data flow perspective for ease in understanding and elucidation.

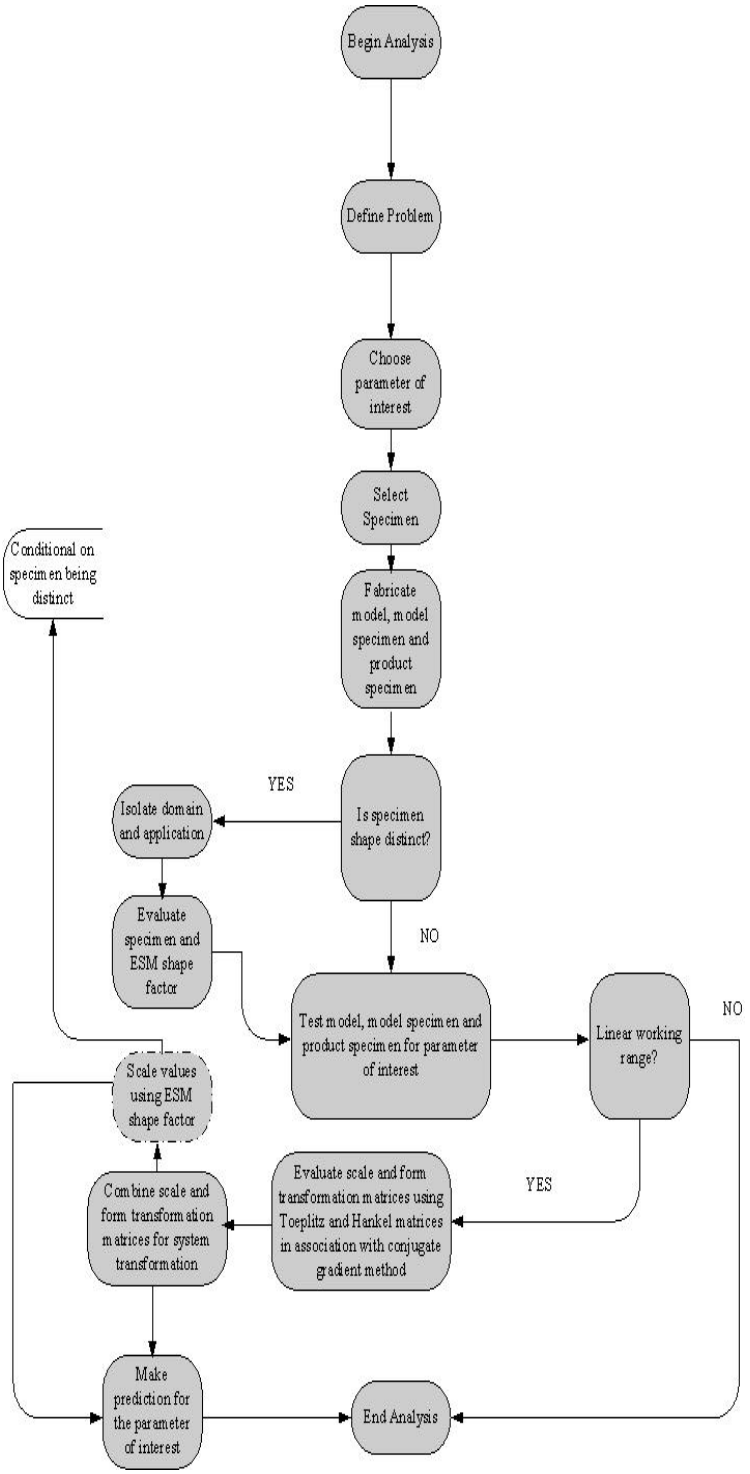

Figure 14. ESM Flow Chart

CONCLUSIONS AND FUTURE WORK

The trends observed from the error plots indicate the robustness of the technique of ESM and the evaluation of different methods from a numerical stand point has opened up numerous avenues for continued research in ESM, most of which are dedicated to applications in product design. Use of special matrices has allowed for increased leverage in terms of mathematical formulation. Employing advanced solution methods has provided immense analytical benefit, an aspect that would hold in good stead when a computational ESM tool or software is conceptualized. The effect of shape factors is another important design consideration that needs to be carefully applied in similitude studies. The ability to choose a specimen and optimize it (for variable shape factors) is a potential extension of the process. The incorporation of such similarity techniques thus holds promise for future designs.

References:

[1] Albert, A., 1972, *Regression and the Moore – Penrose Pseudoinverse*, Academic Press.

[2] Ashby, M. F., 1992, *Materials Selection in Mechanical Design*, Pergamon Press.

[3] Ashby, M. F., 1991, *Materials and Shape*, Acta. Metall. Mater., 39, 1025 – 1039.

[4] Becker E. B., Carey, G. F., Oden, J.T., 1981, *Finite elements*, Prentice-Hall, Englewood Cliffs, NJ.

[5] Bernstein D. S., 2005, *Matrix Mathematics*, Princeton University Press.

[6] Bridgman, P. W. 1931, *Dimensional Analysis*, Yale University Press, New Haven.

[7] Burgess, S. C., 2000, *Shape factors and material indices for dimensionally constrained structures – Part* 1: *beams*, Proceedings of the Institute of Mechanical Engineers, Vol. 214, Part C, 371 – 379.

[8] Burgess, S. C., 2000, *Shape factors and material indices for dimensionally constrained structures – Part* 2: *shafts*, Proceedings of the Institute of Mechanical Engineers, Vol. 214, Part C, 381 – 388.

[9] Burgess, S. C., Kahangamage, U. P., Barr, G., Williams, J. S., 2001, *Shape factors for beams with misaligned loads*, Proceedings of the Institute of Mechanical Engineers, Vol. 215, Part C, 981 – 993.

[10] Cho, U., and Wood, K., 1997, "Empirical Similitude Method for the Functional Test with Rapid Prototypes," *Proceedings of the Solid Freeform Fabrication Symposium*, Austin TX, September, 1997, pp. 559 – 567.

[11] Cho, U., Wood, K. L., and Crawford, R. H., 1998b, "Novel empirical similarity method for the reliable product test with rapid prototypes," *Proceedings of DETC*, Atlanta, GA, September 13 – 16, 1998.

[12] Cho, U., Wood, K. L., and Crawford, R. H., 1998, "Online Functional Testing with Rapid Prototypes: a Novel Empirical Similarity Method," *Rapid Prototyping Journal*, 4, No. 3, pp. 128 – 138.

[13] Cho, U., 1999, *Novel Empirical Similarity Method for Rapid Product Testing and Development*, Doctoral dissertation, The University of Texas at Austin.

[14] Davis, P. J., 1979, *Circulant Matrices*, A Wiley - InterScience Publication, John Wiley & Sons.

[15] Dutson, A.J, 2002, *Functional Prototyping Through Advanced Similitude Techniques*, Doctoral dissertation, The University of Texas at Austin.

[16] Gere, J. M., Timoshenko, S. P. , 1985, *Mechanics of Materials*, Wadsworth International, London.

[17] Golub, G. H., Van Loan, C. F. , 1996, *Matrix computations*, 3rd edition, Baltimore, Johns Hopkins.

[18] Grenander, U., Szegö, G., 1958, *Toeplitz Forms and their Applications*, University of California Press, Berkeley and Los Angeles.

[19] Harper, C.A., 2005, *Electronic Packaging and Interconnection Handbook*, 4th Edition, McGraw – Hill.

[20] Hestenes, Magnus R., Stiefel, Eduard, 1952, *Methods of Conjugate Gradients for Solving Linear Systems*, Journal of Research of the National Bureau of Standards 49 (6).

[21] Incropera F.P., 2007, *Fundamentals of heat and mass transfer*, 6th ed, John Wiley, Hoboken, NJ.

[22] Jones K.W., Liu Y., Shah M., Clarke R., 1998, *Mechanical properties of Pb/Sn Pb/In and Sn-In Solders*, Soldering & Surface Mount Technology, Volume 10 Number 1, 37 – 41.

[23] Langhaar, H. L., 1951, *Dimensional Analysis and Theory of Models*, John Wiley & Sons, New York.

[24] Murphy, G., 1950, *Similitude in Engineering*, The Ronald Press Company, New York.

[25] Ng, M. K., 2004, *Iterative Methods for Toeplitz Systems*, Oxford Science Publications, New York.

[26] Pecht, M.A., Agarwal, R., McCluskey, P., Dishnogh, T., Javadpour, S., Mahajan, R., 1999, *Electronic Packaging: Materials and Their Properties*, CRC Press.

[27] Peller, Vladimir V., 2003, *Hankel operators and their applications*, Springer – Verlag, New York.

[28] Penrose, Roger, 1955, *A generalized inverse for matrices*, Proceedings of the Cambridge Philosophical Society 51, 406-413.

[29] Rayleigh, 1915, *The Principle of Similitude*, Nature, No. 2368, Vol. 95, 66 – 68.

[30] Roark, R. J., Young, W. C. , 1976, *Formulas for Stress and Strain*, 5th edition, McGraw Hill, London.

[31] Robinson, E.A., 1981, *Least Squares Regression Analysis in terms of Linear Algebra*, Goose Pond Press, Houston.

[32] Shewchuk, J. R., 1994, *An Introduction to the Conjugate Gradient Method Without the Agonizing Pain*, Edition $1\frac{1}{4}$, School of Computer Science, Carnegie Mellon University Pittsburgh, PA.

[33] Skoglund, V.J., 1967, *Similitude – Theory and Applications*, International Textbook Company, PA.

[34] Szirtes, T., 1998, *Applied Dimensional Analysis and Modeling*, McGraw – Hill, New York.

[35] Wood, J. J., and Wood, K. L. 2002b. "Empirical Analysis using Advanced Similarity Methods," *Proceedings of DETC*, Montreal, Canada, 2002, pp. 429 – 438.